Environ. Sci. Technol. **2006**, *40,* 2262−2268

Evidence of a Stable Uranyl Site in Ancient Organic-Rich Calcite

SHELLY D. KELLY,*,† E. TROY RASBURY,‡ SOMA CHATTOPADHYAY,† A. JEREMY KROPF,† AND KENNETH M. KEMNER†

Argonne National Laboratory, Argonne, Illinois 60439, and SUNY Stony Brook, Stony Brook, New York 11794

The mechanism of uranium (U) incorporation into calcite (calcium carbonate) is of fundamental importance to the fate and transport of U at the surface and in the shallow subsurface and has implications for (a) the accuracy of U−Pb and U-series isotope ratio methods used to determine the ages of ancient deposits and (b) potential remediation strategies based on sequestration of U in the subsurface. Extended X-ray absorption fine structure (EXAFS) spectroscopy is uniquely suited to the study of U−calcite systems. The sensitivity of the EXAFS spectrum to the local atomic Ca coordination about U(VI) in the calcite structure results in an increase in the number and amplitude of Ca signals as the U(VI) becomes more ordered within the crystal structure. Our X-ray microprobe (10-μm) measurements of an ancient 298 million-year-old organic-rich calcite (calcrete) clearly revealed three coordination shells of Ca atoms, defining a well-ordered calcite structure about uranyl to a distance of ∼6.5 Å. These results indicate that uranyl is incorporated at the Ca^{2+} site in calcite and that the uranyl environment may evolve over long time scales, becoming more calcite-like and more stable for long-term sequestration of uranium. These results therefore validate U-related dating methods and show that calcite can be effective at sequestering U in vadose zone sediments.

Introduction

Knowledge of the incorporation of hexavalent U, U(VI), into calcite would lend confidence in U−Pb and U-isotope-series dating of natural calcite (including calcretes) and could identify an effective mechanism for long-term sequestration of U(VI). Calcretes are calcium carbonate deposits that are formed in near-surface environments. Calcretes can form in the vadose zone (pedogenic type), as well as at or near the water table (groundwater type). The calcite formed in these deposits records the integrated history of the fluids responsible for formation of the deposits, along with any possible diagenetic changes. Hence, the constituents of calcretes can be very sensitive probes of conditions at the time of calcrete formation (*1*). Calcretes have been exploited for paleo-pCO_2 studies (*2*) and recently for both U−Pb (*3*−*5*) and U-isotope-series (*6*−*9*) dating of the time of surface exposure. The unsubstantiated U−Pb and U-isotope-series dating methodologies assume that U is incorporated into calcite when the calcite is formed and that U is not replaced or displaced by weathering processes over millions of years. The integrated ancient history preserved in the structure and chemical composition of calcretes can provide valuable insight into the behavior of U in calcite in vadose zone sediment; this is of great interest in nuclear waste handling and remediation of U-contaminated subsurface environments. Successful U remediation strategies focused on sequestering U within the subsurface to prevent the migration of U to groundwater supplies require knowledge of the potential mobility of U(VI). Definitive determination of the structure of U(VI) incorporated into calcite has heretofore been impossible, and therefore the potential mobility of U(VI) in calcite formations has not been understood.

U(VI) has been shown to be taken up by calcite, but the mechanism remains elusive (*10*, *11*). Only one study has given spectroscopic evidence for substitution of U(VI) for Ca^{2+} within the calcite structure, probably through initial incorporation from the aragonite phase (*12*). The soluble form of U, U(VI), is often associated with two tightly bound axial oxygen atoms (O_{ax}), forming a linear uranyl (UO_2^{2+}) moiety that differs in size and shape from the Ca^{2+} cation found in calcite ($CaCO_3$) host rock. These differences have led many to conclude that the uranyl cation cannot substitute for Ca^{2+} and still preserve the calcite structure (*13*, *14*).

Extended X-ray absorption fine structure (EXAFS) measurements have been instrumental in studies of U in solid and aqueous phases with calcium and carbonate, with sensitivities approaching environmentally relevant U concentrations of ∼1−10 mg kg^{-1}. Previous work has shown that U(VI) in a natural 13 700-year-old (13.7-ka) U-rich calcite ([U] ≈ 360 mg kg^{-1}), initially formed from an aragonite phase, is coordinated by 6 Ca atoms at a distance consistent with the substitution of uranyl into a Ca-like site (*12*). The 13.7-ka calcite may be unique with regard to the incorporation of U(VI), because it was transformed from aragonite to calcite and contains relatively high [U]. In laboratory studies, aragonite and calcite have been synthesized in the presence of higher U(VI) concentrations, approaching 1000 mg kg^{-1} in the solids (*14*, *15*). The synthetic aragonite was shown to accommodate U(VI) with little distortion to the uranyl triscarbonate aqueous species (*5*, *6*). In contrast, the synthetic calcite contained a disordered U(VI) atomic environment, as evidenced by the absence of coordinating Ca atoms. The disordered U(VI) in synthetic calcite probably increases the solubility of the calcite (*14*, *15*). The aragonite precursor of the natural 13.7-ka calcite might have facilitated the incorporation of U(VI) into this natural calcite. The other common U oxidation state, U(IV), has been shown to be substituted in the Ca site in calcite, with uniform first-oxygen coordination and [U] = 5−35 mg kg^{-1} (*16*). In the aqueous phase, EXAFS spectroscopy was used to identify Ca coordinated to aqueous uranyl triscarbonate, forming an aqueous $Ca-UO_2-CO_3$ species at an environmentally relevant [U] = 50 μM (*17*). This aqueous species is credited with increasing the mobility of U(VI) (*18*, *19*) and decreasing the availability of U(VI) for microbial reduction (*17*). These studies highlight the importance of the interaction between Ca^{2+} and CO_3^{2-} in controlling the bioavailability and geochemistry of U in groundwaters and vadose zone sediments.

These studies set the stage for determination of the U(VI) coordination environment at naturally occurring concentrations in an ancient calcite (calcrete) formed near the water table and exposed to organic matter and bioreducing conditions. The objective of this study is to determine the local atomic environment and oxidation state of U in a natural

* Corresponding author phone: (630)252-7376; fax: (630)252-9793; e-mail: skelly@anl.gov.
† Argonne National Laboratory.
‡ SUNY Stony Brook.

10.1021/es051970v CCC: $33.50

Published on Web 03/08/2006

298 million-year-old (298-Ma) calcrete ([U] = 6−8 mg kg^{-1}). Our EXAFS spectrum is consistent with U(VI) fully incorporated into the calcite structure, indicating that calcite can accommodate U(VI) without significant distortion of the host calcite to form a stable environment for long-term sequestration of U. These results therefore validate U-related dating methods and provide an alternate strategy for the long-term sequestration of U in the subsurface.

Samples and Experimental Methods

298-Ma Calcrete. Here, we focus on a calcrete sample that is precisely dated at 298 ± 1 Ma and shows no evidence of loss of U on this very long time scale (*3*, *4*). On the basis of several lines of evidence, this calcrete has been interpreted as having formed near the water table, with some exposure to a reducing environment (*20*). Additional information about the calcrete specimen can be found in the Supporting Information. An optical image of a polished slab of the calcrete is shown in Figure 1A. The 1-cm × 1-cm × 0.8-cm piece of calcrete was used for all X-ray absorption measurements at room temperature, without modification of the original sample.

X-ray Measurements. The microprobe X-ray measurements were made at the Materials Research Collaborative Access Team (MR-CAT) sector 10-ID beamline (*21*) at the Advanced Photon Source. The MR-CAT beamline setup parameters are given in the Supporting Information. Caution is needed in comparing the optical image to the X-ray fluorescence (XRF) image because of differences in penetration depth. The penetration depth of the X-rays (~4-mm) results in an apparent X-ray microprobe size of approximately 16 μm (see Supporting Information). To increase the probability of finding a region of the sample with a U concentration in the range of our measurement capabilities, we did not reduce the thickness (0.8 cm) of the original sample. As a result, the X-ray optical image does not compare as well with the X-ray fluorescence (XRF) image, and we have lost some of the spatial resolution provided by the Kirkpatick−Baez mirrors. The use of the thick sample was considered acceptable, because the spatial resolution and the correspondence of the optical image with the XRF image are not critical to the measurement.

Valence State Methods. At least two different methods can be used with the X-ray microprobe to determine the spatial distribution of U(VI) to U(IV) in the sample. The most robust method would involve scanning the energy of the X-ray probe a few hundred electronvolts on either side of the U absorption edge and using the entire shape of the absorption curve to determine the U valence distributions. Figure S2 shows the entire microprobe X-ray absorption near-edge spectra (μXANES) for our calcrete sample at one location, a U(VI) standard, and a U(IV) standard. Measuring μXANES spectra across the entire adsorption edge to determine the U oxidation state in ~200 sampled regions in the calcrete with various total U concentrations would require a prohibitively long collection time of about 30 h. Therefore, we measured the absorption coefficient at three energy values to reduce the collection time to approximately 2 h for all ~200 sampled regions. A description of these three energy values can be found in the Supporting Information.

***μ*EXAFS Data Processing.** Details of the microprobe X-ray absorption fine structure (μEXAFS) data processing can be found in the Supporting Information. Thirty μEXAFS measurements were made at the position identified from U μXRF distributions. The resulting averaged $\chi(k)$ data are shown in Figure S2.

The U L_{III}-edge μEXAFS data from the calcrete sample were modeled with many different possible uranyl coordination environments, including O, C, P, Fe, Ca, and U neighboring atoms at several distances, as well as several uranyl crystal structures, including schoepite, rutherfordine, andersonite, and liebigite. More than 50 different uranyl coordination environments were explicitly tested. Only the best-fit model is shown, as all other models were judged

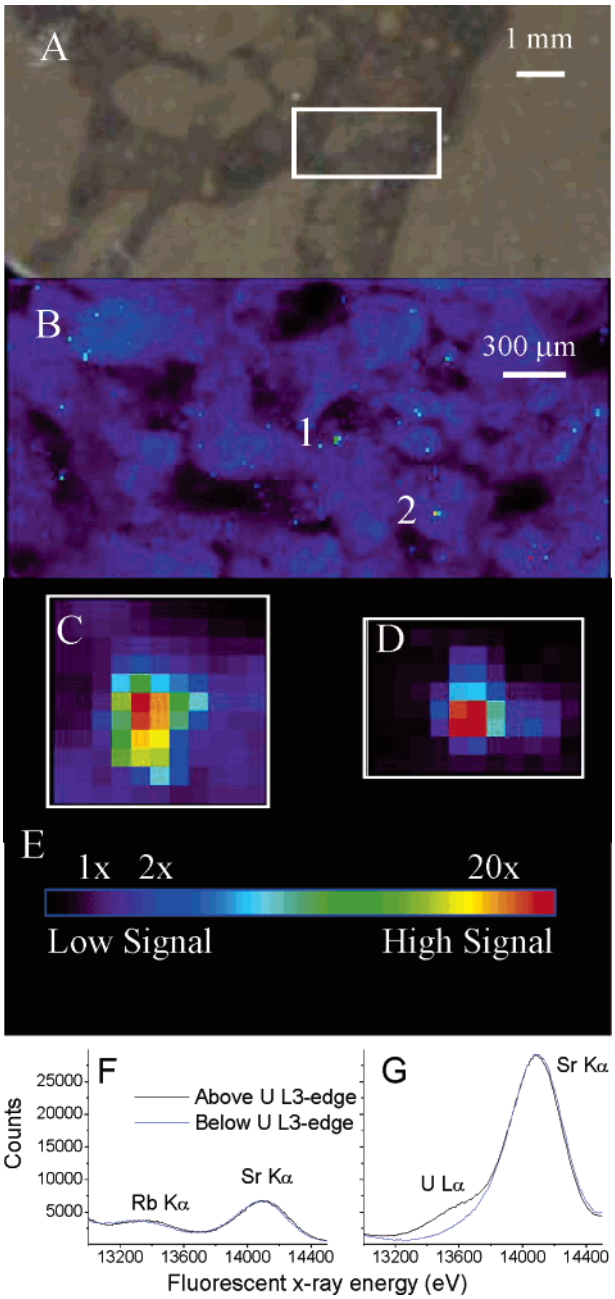

FIGURE 1. Images of calcrete sample. (A) Optical image. The white box represents a 3-mm × 1.4-mm area scanned with an X-ray microprobe effectively 16 μm × 16 μm. (B) Spatial distribution of the X-ray fluorescence (XRF) intensity (without background subtraction) within the energy range of the U Lα signal (13 250−13 725 eV). (C and D) Spatial distributions of the XRF intensity in two regions of elevated XRF intensity labeled 1 and 2, respectively, in panel B. (E) Color bar representing low to high XRF intensity. The maximum XRF intensity (red squares) and mean signals (blue squares) are approximately 20 and 2 times the minimum XRF intensity (black squares), respectively. (F and G) XRF spectra from the elevated XRF regions shown in panels C and D, respectively. Each point shown in panels B, C, and D represents the U XRF intensity integrated for 3 s over the energy range 13 250−13 725 eV, with spacings of 20 μm × 20 μm, 10 μm × 10 μm, and 10 μm × 10 μm between points, respectively, and an incident X-ray beam cross section of 16 μm × 16 μm.

unacceptable on the basis of nonphysical parameters or an inability to reproduce the measured spectrum. The data range (2.3−8.2 $Å^{-1}$) and the fit range (1−6 Å) correspond to 20 independent points. A justification for using the fit range 1−6 Å can be found in the Supporting Information.

Results and Discussion

Compilation of XANES Standards. The average valence state of U within the sample was determined by calibrating the normalized absorption coefficient μ_v measured above the U L_{III}-edge at 17 200 eV to a series of standards, rather than by measuring the entire absorption edge at each sampled region. We compiled normalized U L_{III}-edge X-ray absorption near edge spectra (XANES) for six U(VI)−uranyl samples, two U(VI) uranate samples, three U(IV) samples, and one sample with a mixture of U(VI) and U(IV) (Figure S3). These spectra were collected from a variety of solids, aqueous solutions, and pastes, as detailed in Table S2. The X-ray absorption coefficients at the valence state contrast energy $[\mu_v = \mu(XRF_v) - \mu(XRF_{bkg})]/[\mu(XRF_t) - \mu(XRF_{bkg})]$ for these data, and also for two additional uranate samples of U(VI) without the typical uranyl moiety, are listed in Table S2. The X-ray absorption coefficient at the contrast energy is enhanced by multiple scattering from the O_{ax} atoms of the uranyl moiety for U(VI) versus U(IV). In addition, Table S2 shows that uranate [U(VI) without the typical O_{ax} bonding] shows unique absorption at this energy (average $\mu_v = 1.02 \pm 0.02$) that is slightly smaller than typical values for uranyl (average $\mu_v = 1.08 \pm 0.03$) but larger than typical values for U(IV) (average $\mu_v = 0.90 \pm 0.04$). By choosing the contrast energy value above the adsorption edge, we gain information about the valence state of U and some information about the uranyl binding environment (i.e., uranyl as compared to uranate).

Previously, the contrast energy value was chosen to be at the absorption edge, relying on the shift in the absorption edge of U(VI) and U(IV) to determine the valence state ratio (*23*). At this energy, the absorption coefficient changes rapidly for both U(VI) and U(IV). As a result, small shifts in incident X-ray energy during the measurement are interpreted as changes in the ratio of U(VI) to U(IV). Instead, for this work, we chose to use the resonance feature above the adsorption edge at 17 200 eV to determine the U valence state ratio, as demonstrated previously for other systems (*24*). The absorption coefficient does not change rapidly at this energy. Thus, in theory, any error due to a slight energy shift should be small.

***μ*XRF.** Microprobe X-ray fluorescence (μXRF) measurements (16-μm resolution) were made on the calcrete sample without additional modification. A dark, 3-mm × 1.4-mm region of the calcrete investigated with the X-ray microprobe is outlined by the rectangle drawn on the optical image in Figure 1A. The spatial distribution of the XRF intensity in this region, corresponding to U and/or Sr and/or Rb, is shown in Figure 1B. Two regions in Figure 1B with elevated XRF intensities (red to orange) had ∼20 times the XRF intensities of the lowest signals measured (black). The fine-scale spatial distributions in these regions are shown in Figure 1C and D. These false-color images are scaled as shown by the color bar in Figure 1E. Qualitatively, the black to red regions represent low to high XRF intensity. Energy-dependent XRF spectra, collected with X-ray probe energies above and below the inner-shell electron binding energy (L_{III}-edge) of U, to determine the elemental source of the elevated XRF signal, are shown in Figure 1F and G. These spectra demonstrate that the elevated XRF intensity in Figure 1C is due to Rb impurities, as the XRF spectrum does not change above and below the U L_{III}-edge (Figure 1F). The elevated XRF intensity in Figure 1D shows the expected change in the XRF spectra due to the U XRF signal; the μEXAFS data were collected (Figure 1G) from this position.

U Valence State Results. Figure S1 shows the full normalized μXANES spectra for the calcrete at the location shown in Figure 1G, U(VI) in a hydrogen uranyl phosphate standard, and U(IV) in a uraninite standard. The correspondence of the rise in the absorption edges in the calcrete spectrum and the U(VI) standard spectrum confirms that U(VI) is the dominant U oxidation state in the region of the sample probed. The absence of the resonance feature above the edge in the calcrete μXANES spectrum confirms that this U(VI) is uranate, as described previously (*25*, *26*).

The U valence state of a 75-μm × 250-μm region of the calcrete sample (collected with a 10-μm × 10-μm step size, for a total of approximately 200 sampled regions) was determined by collecting the XRF intensities at three different energy values (XRF_{bkg}, XRF_v, and XRF_t), as described in the Experimental Section. Details of the XRF mapping procedures can be found in the Supporting Information.

The μXRF valence state map (Figure 3A) showing the distribution of normalized absorption coefficient at the uranium valence state contrast energy (μ_v) indicates a fairly uniform (yellow to orange) μ_v value of 1.01 ± 0.02. A histogram of the number of occurrences for each value of μ_v within the calcrete sample, shown in Figure 3B, illustrates the Gaussian distribution of μ_v in the calcrete sample, centered at 1.01 ± 0.02. The μ_v values (1.01 ± 0.02) in the calcrete sample are (a) tightly distributed about the values found for other U(VI) samples with relaxed O_{ax} atoms ($\mu_v = 1.02 \pm 0.02$), (b) slightly smaller than the average μ_v value (1.08 ± 0.03) for the U(VI) samples with typical O_{ax} bonding, and (c) greater than typical μ_v values of 0.90 ± 0.04 for U(IV) samples (see Table S2). We interpret these observations as evidence for one dominant uranyl species within the calcrete sample that is similar to the species investigated by the μEXAFS measurements, indicating predominantly U(VI) fully incorporated within the calcite structure, with a nontypical uranyl O_{ax} bonding environment. The nontypical uranate environment of the calcrete is shown by the full μXANES spectra collected with the μEXAFS data (Figure S1).

***μ*EXAFS.** We used μXAFS spectroscopy to determine the average atomic environment of U in the calcrete sample in the region of elevated XRF intensity shown in Figure 1G. The *k*-space and *R*-space U L_{III}-edge μEXAFS data and the best-fit model are shown in Figure S2 and Figure 4, respectively. The normalized XANES spectrum from this same location, shown in Figure S1, indicates U(VI) with a symmetrical uranate-type environment, as discussed previously. The best fit to the μEXAFS spectra was based on uranyl incorporation into calcite, as illustrated in Figure 2. This model is based on the replacement of 1 Ca and 2 carbonate groups (Figure 2A) with 1 U and 2 O_{ax} atoms of the uranyl structure (Figure 2B). For clarity, this figure omits the carbonate groups associated with the axial oxygen atoms. Although our fitting results indicate that only four carbonate groups are bound to the uranyl, the model does not require a decrease in the number of carbonate groups. The EXAFS model and parametrizations are listed in Table S1. The model used the 14 parameters shown in the table in bold type, along with 1 energy shift parameter, for all paths. The model assumed that each equatorial oxygen atom and each carbon atom about the uranyl were associated with a carbonate group. The distribution of parameters for the fitted data range is explicitly justified in the Supporting Information. The best-fit value for the number of carbonate groups (4.3 ± 0.6) is consistent with value of 4 predicted by this model (Table S3).

Table 1 compares the coordination environments of Ca in calcite and U in the 298-Ma calcrete. The best-fit value for the U−C distance of 3.49 ± 0.01 Å represents an expansion by approximately 9% over the Ca−C distance in calcite (3.21 Å). The distances for the next 6 Ca atoms in the calcrete are split into two groups, presumably because of the linear shape

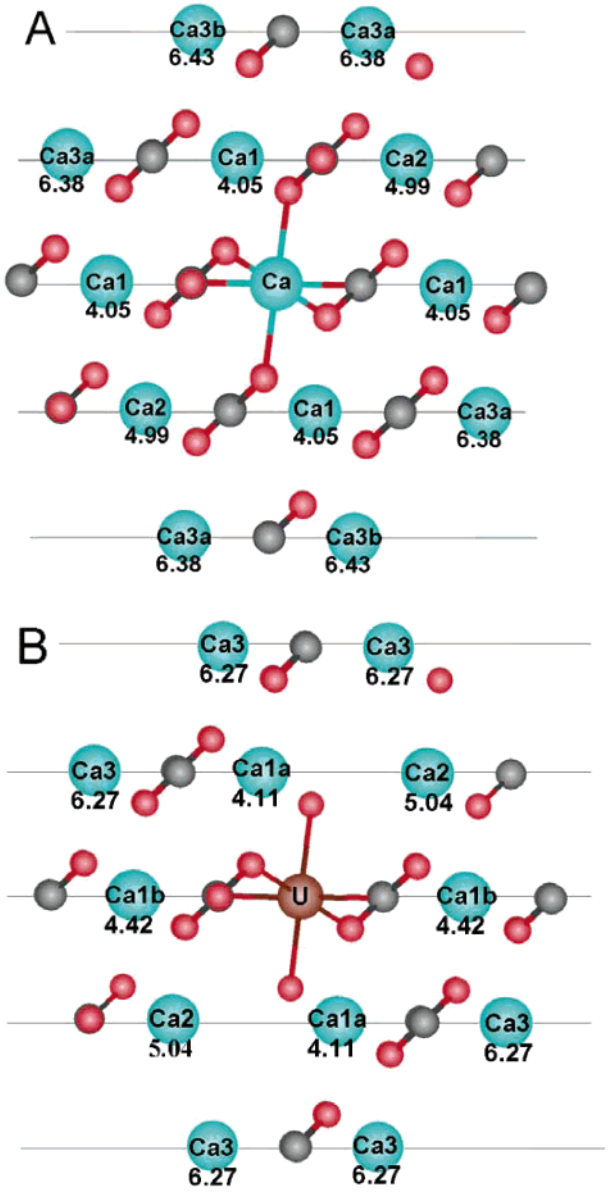

FIGURE 2. (A) Crystallographic representation of the calcite structure with Ca at the center. (B) Crystallographic representation of the uranyl structure within calcite that is consistent with the μEXAFS results, with uranyl replacing the Ca at the center of panel A. The Ca atoms at different distances from the uranyl are labeled. The brown, blue, red, and gray spheres represent U, Ca, O, and C atoms, respectively. The numbers below the labeled atoms correspond to the distances in angstroms to that atom from the central atom. These values for (A) are based on the calcite structure (*22*), and those for (B) are based on the μEXAFS results.

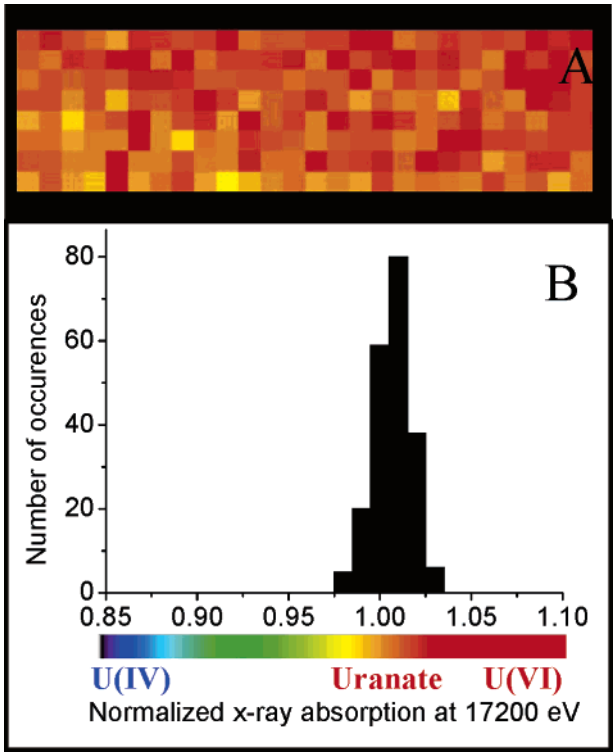

FIGURE 3. μXRF valence state map. (A) Spatial distributions of U valence state in ~200 sampled regions depicted by the XRF intensity ratio $\mu_v = (\mu(XRF_v) - \mu(XRF_{bkg}))/(\mu(XRF_t) - \mu(XRF_{bkg}))$. The normalized absorption coefficient at the valence state contrast energy (μ_v) of the calcrete sample is calibrated to show U(VI) with typical O_{ax} bonding (red), U(VI) with nontypical O_{ax} bonding such as uranate (yellow-orange), and U(IV) (black-blue). The color bar for panel F is at the bottom of panel G. (B) Histogram for panel F, showing the distribution of absorption values at the valence state contrast energy of the calcrete.

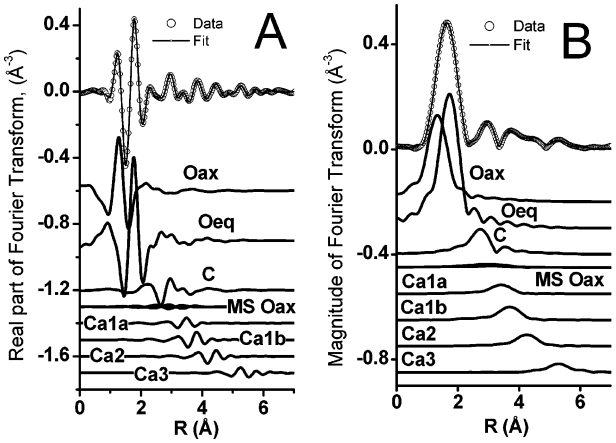

FIGURE 4. Microprobe EXAFS data and model from the calcrete sample. (A) Real part and (B) magnitude of the Fourier transform of the calcrete data (open circles) and the modeled fit to the data (solid line), shown together at the tops of the graphs. The curves below represent the deconvolution of the modeled fit to the data, showing the contribution from each path in the model. This model is based on the corresponding coordination shells of atoms depicted in Figure 2B.

of the uranyl moiety. Of the 6 Ca atoms, 2 have U−Ca distances of 4.11 ± 0.04 Å, similar to the Ca−Ca distance of 4.05 Å in calcite. The remaining 4 Ca atoms from this coordination shell are expanded from this distance by approximately 9%, the same as the expansion for the 4 C atoms shared with uranyl. This expansion of the 4 C atoms of the equatorial carbonate groups results in a relaxation of the carbonate bond angle (U−O_{eq}−C, where O_{eq} is equatorial oxygen) from 121° for Ca−O_{eq}−C to 147° ± 3° for U−O_{eq}−C. In addition, this expansion of the 4 C atoms, plus the expansion of the 4 neighboring Ca atoms that share the carbonate groups, is the total extent of the local distortion introduced into the local crystal structure by the substitution of a uranyl ion for 1 Ca^{2+} ion and 2 carbonate groups. The next two U−Ca coordination shells (6 and 12 Ca atoms with U−Ca distances of 5.04 ± 0.02 and 6.27 ± 0.03 Å, respectively) are all similar to the Ca−Ca coordination numbers and distances for calcite. The carbonate groups at these longer distances (4−6.5 Å) are not included in the μEXAFS model; their small signal was not needed to reproduce the data,

TABLE 1. Radial Distributions of Atoms about Ca in Calcite and U in the 298-Ma Calcrete, with a Comparison of the Changes in Distances

Ca in calcite[a]			U in 298-Ma calcrete			
neighbor	number	distance, Rca (Å)	neighbor	number	distance, Ru (Å)	ΔR (%) (Ru − Rca)/Rca
			O_{ax}	2	1.867 ± 0.004	N/A
O	6	2.36	O_{eq}	4.3 ± 0.6	2.31 ± 0.01	−2 ± 1
C	6	3.21	C	4.3 ± 0.6	3.49 ± 0.01	9 ± 1
			Ca_{1a}	2.0 ± 0.4	4.11 ± 0.04	1 ± 2
Ca_1	6	4.05	Ca_{1b}	4.0 ± 0.6	4.42 ± 0.04	9 ± 1
Ca_2	6	4.99	Ca_2	6	5.04 ± 0.02	1 ± 1
Ca_{3a}	6	6.38				−2 ± 1
Ca_{3b}	6	6.43	Ca_3	12	6.27 ± 0.03	−2 ± 1

[a] Based on the crystal structure of calcite, ref *22*.

because the EXAFS signal is proportional to the degeneracy and the electron density of the atoms. Thus, C and O atoms often are not detected in these EXAFS data beyond 4 Å. Schematics of the local atomic coordination about Ca in calcite (from the crystal structure of calcite) and about U in the calcrete sample (from the μEXAFS data) (Figure 2) provide strong evidence that uranyl occupies a Ca site within the calcite structure, with minimal distortion to the host calcite.

Axial Oxygen Atoms of Uranyl. Microprobe X-ray absorption near-edge structure (μXANES) spectra clearly identify U(VI) at the investigated location (Figure S1). Additional μXANES measurements in 200 sampled regions of the calcrete (each 16 μm × 16 μm) confirmed the presence of U(VI) (Figure 3). These measurements also demonstrated that all sampled regions have unique spectra related to the uranate-like structure of the uranyl moiety. This structure is elucidated by μEXAFS results showing that the U−O_{ax} bond in the 298-Ma calcrete is weakened (as indicated by its large σ^2 value) and lengthened as compared to the bond in typical uranyl species. This leads to a single first shell peak in the magnitude of the Fourier transform corresponding to the axial and equatorial atoms. (Signal content in the EXAFS spectrum is described in the Supporting Information.) The uranyl environment in this 298-Ma calcrete is unique. Our U−O_{ax} bond length of 1.87 Å is 0.08 Å longer than the average U−O_{ax} bond length (1.79 Å), as determined for 93 different typical uranyl environments (*27*). This longer U−O_{ax} bond length is common for the uranate species. For example, four different cesium uranate minerals have been shown to have U−O_{ax} bond lengths ranging from 1.78 to 1.96 Å (*26*). The average U−O_{ax} bond length for these four minerals is 1.91 Å, greater than the U−O_{ax} bond length of 1.87 Å for this 298-Ma calcrete. In the previous study, U−O_{ax} bonds were defined as less than 2.0 Å, while U−O_{eq} bonds were defined as greater than 2.0 Å. Uranate structures show a symmetrical uranium environment (*26*). These uranate species give a XANES spectrum that is similar to our XANES spectrum (Figure S1), which is missing the resonance feature above the adsorption edge. Unfortunately, these data were not analyzed to serve as a reference for our σ^2 value for the U−O_{ax} bond. In another study, U(VI) oxide precipitates exhibited increasing U−O_{ax} bond length with increasing pH of formation. At pH 11, EXAFS analysis showed a U−O_{ax} bond length of 1.86 ± 0.02 Å (*28*), similar to our bond length of ∼1.87 Å. This study found a σ^2 value of ∼0.004 Å^2 for the U−O_{ax} bond length, which is smaller than our value of ∼0.013 Å^2. This discrepancy is not surprising, given that the XANES spectrum from the pH 11 precipitate shows the resonance feature that is not apparent for our 298-Ma calcrete sample (Figure S1), as discussed above.

Previous theoretical calculations of U L_{III}-edge XANES spectra for U(VI) (*29*) showed that the resonant feature above the edge of a typical uranyl species (Figure S2) is due to multiple scattering paths of uranyl. The absence of this resonant feature in the calcrete XANES spectrum is due to lengthening and weakening (increased σ^2-value) of the U−O_{ax} bond, as shown by the μEXAFS results. In addition, this particular U(VI) species has a unique μXANES spectrum detected in more than 200 sampled regions of the calcrete. Bulk luminescence data (*20*) collected from this sample also show a unique spectrum similar to that of a uranate U(VI) in apatite (*25*), U(VI) without the O_{ax} atoms of the uranyl, consistent with relaxation of the uranyl bonding environment in this calcrete. Other recent studies have shown that when the O_{ax} atoms of uranyl participate in bonding with other atoms, like those found in organics, the O_{ax} bond is weakened (*30*).

The bulk luminescence measurements, ∼200 independent μXANES measurements (away from the U-rich regions of the calcrete), and μEXAFS measurements (in a U-rich region of the calcrete) all support the conclusion that sterically demanding ligands within the calcite structure give nontypical uranyl (i.e., uranate) coordination geometry, resulting in distortion of the uranyl bonding. This is strong evidence that the uranyl structure reported is representative of the calcrete sample in all of these regions.

Charge Balance. Previous studies of trace metal substitution for Ca^{2+} in calcite and other mineral structures have shown that the ability of a host mineral to take up the impurity depends on the size and the charge of the impurity (*31*). Our EXAFS results indicate that the uranyl in this natural calcrete is coordinated by four carbonate groups about the equatorial plane. Two additional carbonate groups in the calcite structure that should be in the positions of the O_{ax} atoms of the uranyl were not detected. The two likely explanations are that these two carbonate groups are (a) randomly orientated or (b) completely missing and replaced by other impurities. Thus, the reason for the decreased coordination cannot be determined. For example, if carbonate groups are removed completely, a charge imbalance is created by the substitution of uranyl for a Ca^{2+} ion and two carbonate groups, with a net change in charge of −4. Thus, if carbonate groups are missing, uranyl cannot be incorporated into the structure without additional accommodation of charge by impurities.

Implications for U(VI) Stability in Calcite. The uraniferous rhizoliths of the 298-Ma calcrete might be explained in terms of microbially induced mineralization. The positive correlation between (a) U-rich areas of the calcrete sample with organic matter (see Figure 1 and ref *20*) and (b) enhanced microbial activity (see Supporting Information and ref *20*) implies that biological processes, organic matter, or both may have facilitated the incorporation of uranyl into the calcite structure or controlled calcite growth. Organic matter has been implicated as accounting for crystal morphologies seen in epitaxial overgrowths on needle fiber calcite (*32*). No organic matter bound to U was detected in the U μEXAFS

data, either because the material is highly disordered or because it has been degraded and is not bound to U.

The oxidation state of U in this 298-Ma calcrete has not been altered by digenesis effects, on the basis of the preserved structures within the calcrete (*4*). Although U(VI) is readily reduced to U(IV) under bioreducing conditions (*33*, *34*), the microprobe measurements (Figure S1 and Figure 3) clearly indicate that U in this calcrete is incorporated largely as U(VI). However, U(VI) in the presence of calcium carbonate forms a stable uranyl−triscarbonate−calcium (UO_2−CO_3−Ca) aqueous complex that is resistant to microbial reduction (*17*). Thus, although evidence indicates that bioreducing conditions were present during the formation of this calcrete, the UO_2–CO_3−Ca complex might have been a precursor for incorporation of U(VI) rather than U(IV) into the calcite structure. Previous studies have shown that the uranyl−triscarbonate−calcium complex can be adsorbed to the surface of calcite; this condition could be a precursor for incorporation (*35*).

Differences between the uranyl local structure of previously characterized synthetic calcite (*14*, *15*), previously characterized 13.7-ka calcite (*12*), and the 298-Ma calcrete we studied might be explained in terms of the change in geometry of uranyl from the aqueous phase to the solid phase. Although these calcites formed under different conditions, they are indeed similar in the sense that they all represent U(VI) in solid phases closely associated with the calcite crystal structure. The likely aqueous uranyl species in this system is the uranyl triscarbonate (with or without Ca bound to the uranyl triscarbonate, as noted previously). This species is 8-fold coordinated, with 2 axial oxygen atoms and 6 equatorial oxygen atoms (from the 3 carbonate groups) forming a hexagonal bipyramidal structure, while uranyl in the calcite structure is 6-fold coordinated, forming a square bipyramidal structure. Uranyl minerals have been shown to exhibit both hexagonal and square bipyramidal geometries (*27*); such a change in geometry could accompany uranyl incorporation at the Ca^{2+} site in the calcite structure. The notable structural differences between uranyl in artificially synthesized calcite (*14*, *15*), a previously studied 13.7-ka uranyl in calcite (*12*), and the 298-Ma uranyl in calcite that we studied are (a) the increasing signals in the investigated sequence of 0 to 6 to 24 distant Ca atoms, respectively, and (b) the relaxation of the U−O_{ax} bond of the uranyl in the 298-Ma sample as compared to the other two samples. Although we have no proof of mechanism, we speculate that the passage of time and direct or indirect effects of biological processes enabled uranyl to be more fully incorporated in the 298-Ma calcite structure, accounting for the ordering of the distant Ca shells about the uranyl and the relaxation of the U−O_{ax} bonds. Comparison of our results to previous results suggests that the uranyl environment evolves over long time scales, becoming more calcite-like and more stable for long-term sequestration of uranium.

Understanding the conditions required for the structural incorporation of U(VI) into calcite is not trivial. This study shows that, in some natural settings, uranyl is structurally incorporated into calcite. Differences in the local atomic environment of U in calcite from different samples likely reflect the evolution of the structure over time, becoming more calcite-like and more stable for long-term sequestration of uranium. The robust U−Pb age of our very ancient sample suggests that encapsulation of oxidized U(VI) in soil calcite provides a reliable mechanism for long-term sequestration of U. Future remediation strategies for some U-contaminated subsurface environments containing reducible and nonreducible forms of U(VI) might employ sequestration of the nonreducible U(VI) in calcite.

Acknowledgments

We thank Bruce Ravel (Argonne National Laboratory), Edward O'Loughlin (Argonne), Neil Sturchio (University of Illinois at Chicago), and Rich Reeder (SUNY Stony Brook) for helpful suggestions and critical reviews of the manuscript. Our work is supported by the Environmental Remediation Science Program, Office of Biological and Environmental Research, Office of Science, U.S. Department of Energy (DOE), under contract W-31-109-Eng-38. Work at the Advanced Photon Source is supported by the DOE Office of Science, Office of Basic Energy Sciences. The Materials Research Collaborative Access Team (MRCAT) operations are supported by DOE and the MRCAT member institutions.

Supporting Information Available

Additional description of calcrete specimen, MR-CAT beamline parameters, penetration depth of X-ray microprobe, description of three energy values for XRF XANES measurements, details of EXAFS data processing, justification of modeled EXAFS data range, justification of the number of variables in the EXAFS model, details of XRF mapping procedures, and signal content in the EXAFS spectrum. Two tables and four figures. This material is available free of charge via the Internet at http://pubs.acs.org.

Literature Cited

(1) Richards, D. A.; Dorale, J. A. *Uranium-Series Geochemistry*; Mineralogical Soc. America: Washington, 2003; Vol. 52, pp 407−460.
(2) Cerling, T. E. The stable isotopic composition of modern soil carbonate and its relationship to climate. *Earth Planet. Sci. Lett.* **1984**, *71*, 229−240.
(3) Rasbury, E. T.; Hanson, G. N.; Meyers, W. J.; Saller, A. H. Dating of the time of sedimentation using U−Pb ages for paleosol calcite. *Geochim. Cosmochim. Acta* **1997**, *61*, 1525−1529.
(4) Rasbury, E. T.; Hanson, G. N.; Meyers, W. J.; Holt, W. E.; Goldstein, R. H.; Saller, A. H. U−Pb dates of paleosols: Constraints on late Paleozoic cycle durations and boundary ages. *Geology.* **1998**, *26*, 403−406.
(5) Wang, Z. S.; Rasbury, E. T.; Hanson, G. N.; Meyers, W. J. Using the U−Pb system of calcretes to date the time of sedimentation of elastic sedimentary rocks. *Geochim. Comochim. Acta* **1998**, *62*, 2823−2835.
(6) Sharp, W. D.; Ludwig, K. R.; Chadwick, O. A.; Amundson, R.; Glaser, L. L. Dating fluvial terraces by Th-230/U on pedogenic carbonate, Wind River Basin, Wyoming. *Quat. Res.* **2003**, *59*, 139−150.
(7) Ludwig, K. R.; Paces, J. B. Uranium-series dating of pedogenic silica and carbonate, Crater Flat, Nevada. *Geochim. Cosmochim. Acta* **2002**, *66*, 487−506.
(8) Candy, I.; Black, S.; Sellwood, B. W.; Rowan, J. S. Calcrete profile development in quaternary alluvial sequences, southeast Spain: Implications for using calcretes as a basis for landform chronologies. *Earth Surf. Processes Landforms* **2003**, *28*, 169−185.
(9) Blisniuk, P. M.; Sharp, W. D. Rates of late quaternary normal faulting in central Tibet from U-series dating of pedogenic carbonate in displaced fluvial gravel deposits. *Earth Planet. Sci. Lett.* **2003**, *215*, 169−186.
(10) Russell, A. D.; Emerson, S.; Nelson, B. K.; Erez, J.; Lea, D. W. Uranium in foraminiferal calcite as a recorder of seawater uranium concentrations. *Geochim. Cosmochim. Acta* **1994**, *58*, 671−681.
(11) Russell, A. D.; Emerson, S.; Mix, A. C.; Peterson, L. C. The use of foraminiferal uranium/calcium ratios as an indicator of changes in seawater uranium content. *Paleoceanography* **1996**, *11*, 649−663.
(12) Kelly, S. D.; Newville, M. G.; Cheng, L.; Kemner, K. M.; Sutton, S. R.; Fenter, P.; Sturchio, N. C.; Spotl, C. Uranyl incorporation in natural calcite. *Environ. Sci. Technol.* **2003**, *37*, 1284−1287.
(13) Langmuir, D. Uranium solution−mineral equilibria at low temperatures with applications to sedimentary ore deposits. *Geochim. Cosmochim. Acta* **1978**, *42*, 547−569.
(14) Reeder, R. J.; Nugent, M.; Lamble, G. M.; Tait, C. D.; Morris, D. E. Uranyl incorporation into calcite and aragonite: XAFS and luminescence studies. *Environ. Sci. Technol.* **2000**, *34*, 638−644.

(15) Reeder, R. J.; Nugent, M.; Tait, C. D.; Morris, D. E.; Heald, S. M.; Beck, K. M.; Hess, W. P.; Lanzirotti, A. Coprecipitation of uranium(VI) with calcite: XAFS, micro-XAS, and luminescence characterization. *Geochim. Cosmochim. Acta* **2001**, *65*, 3491−3503.
(16) Sturchio, N. C.; Antonio, M. R.; Soderholm, L.; Sutton, S. R.; Brannon, J. C. Tetravalent uranium in calcite. *Science* **1998**, *281*, 971−973.
(17) Brooks, S. C.; Fredrickson, J. K.; Carroll, S. L.; Kennedy, D. W.; Zachara, J. M.; Plymale, A. E.; Kelly, S. D.; Kemner, K. M.; Fendorf, S. Inhibition of bacterial U(VI) reduction by calcium. *Environ. Sci. Technol.* **2003**, *37*, 1850−1858.
(18) Wan, J. M.; Tokunaga, T. K.; Brodie, E.; Wang, Z. M.; Zheng, Z. P.; Herman, D.; Hazen, T. C.; Firestone, M. K.; Sutton, S. R. Reoxidation of bioreduced uranium under reducing conditions. *Environ. Sci. Technol.* **2005**, *39*, 6162−6169.
(19) Dong, W. M.; Ball, W. P.; Liu, C. X.; Wang, Z. M.; Stone, A. T.; Bai, J.; Zachara, J. M. Influence of calcite and dissolved calcium on uranium(VI) sorption to a Hanford subsurface sediment. *Environ. Sci. Technol.* **2005**, *39*, 7949−7955.
(20) McCall, K.; Rasbury, E. T.; Lanzirotti, A.; Tait, C. D.; Donohoe, R. J. Uranyl in organic bearing calcite. In preparation.
(21) Segre, C. U.; Leyarovska, N. E.; Chapman, L. D.; Lavender, W. M.; Plag, P. W.; King, A. S.; Kropf, A. J.; Bunker, B. A.; Kemner, K. M.; Dutta, P.; Druan, R. S.; Kaduk, J. The MRCAT insertion device beamline at the Advanced Photon Source. *Synchrotron Radiat. Instrum.* **2000**, *CP521*, 419−422.
(22) Graf, D. L. Crystallographic tables for the rhombohedral carbonates. *Am. Mineral.* **1961**, *46*, 1283−1316.
(23) Bertsch, P. M.; Hunter, D. B.; Sutton, S. R.; Bajt, S.; Rivers, M. L. In situ chemical speciation of uranium in soils and sediments by micro-X-ray absorption-spectroscopy. *Environ. Sci. Technol.* **1994**, *28*, 980−984.
(24) Ressler, T.; Wienold, J.; Jentoft, R. E.; Neisius, T. Bulk structural investigation of the reduction of MoO_3 with propene and the oxidation of MoO_2 with oxygen. *J. Catal.* **2002**, *210*, 67−83.
(25) Rakovan, J.; Reeder, R. J.; Elzinga, E. J.; Cherniak, D. J.; Tait, C. D.; Morris, D. E. Structural characterization of U(VI) in apatite by X-ray absorption spectroscopy. *Environ. Sci. Technol.* **2002**, *36*, 3114−3117.
(26) Van den Berghe, S.; Verwerft, M.; Laval, J. P.; Gaudreau, B.; Allen, P. G.; Van Wyngarden, A. The local uranium environment in cesium uranates: A combined XPS, XAS, XRD, and neutron diffraction analysis. *J. Solid State Chem.* **2002**, *166*, 320−329.
(27) Bruns, P. C. In *Uranium: Mineralogy, Geochemistry and the Environment*; Burns, P. C., Finch, R., Eds.; Mineralogical Society of America: Washington, DC, 1999; Vol. 38.
(28) Allen, P. G.; Shuh, D. K.; Bucher, J. J.; Edelstein, N. M.; Palmer, C. E. A.; Silva, R. J.; Nguyen, S. N.; Marquez, L. N.; Hudson, E. A. Determinations of uranium structures by EXAFS: Schoepite and other U(VI) oxide precipitates. *Radiochim. Acta* **1996**, *75*, 47−53.
(29) Hudson, E. A.; Rehr, J. J.; Bucher, J. J. Multiple-scattering calculations of the uranium L_3-edge X-ray-absorption near-edge structure. *Phys. Rev. B* **1995**, *52*, 13815−13826.
(30) Sarsfield, M. J.; Helliwell, M.; Raftery, J. Distorted equatorial coordination environments and weakening of U═O bonds in uranyl complexes containing NCN and NPN ligands. *Inorg. Chem.* **2004**, *43*, 3170−3179.
(31) Wood, B. J.; Blundy, J. D. The effect of cation charge on crystal-melt partitioning of trace elements. *Earth Planet. Sci. Lett.* **2001**, *188*, 59−71.
(32) Verrecchia, E. P.; Verrecchia, K. E. Needle-fiber calcite − A critical review and a proposed classification. *J. Sediment. Res., Sect. A* **1994**, *64*, 650−664.
(33) Lovley, D. R.; Phillips, E. J. P.; Gorby, Y. A.; Landa, E. R. Microbial reduction of uranium. *Nature* **1991**, *350*, 413−416.
(34) Suzuki, Y.; Kelly, S. D.; Kemner, K. M.; Banfield, J. F. Enzymatic U(VI) reduction by desulfosporosinus species. *Radiochim. Acta* **2004**, *92*, 11−16.
(35) Rihs, S.; Sturchio, N. C.; Orlandini, K.; Cheng, L. W.; Teng, H.; Fenter, P.; Bedzyk, M. J. Interaction of uranyl with calcite in the presence of EDTA. *Environ. Sci. Technol.* **2004**, *38*, 5078−5086.

Received for review October 4, 2005. Revised manuscript received January 25, 2006. Accepted February 6, 2006.

ES051970V